InSAR Stack Processing — Deformation Mapping in the Area of Northern Bohemia
Proposal for the PhD research

Ing. Ivana Hlaváčová
Department of Mapping and Cartography
Faculty of Civil Engineering
Czech Technical University, Prague
Supervisor: Doc. Ing. Lena Halounová, CSc.

Abstract

Radar interferometry is a method providing a possibility to map deformation in an area imaged by a satellite carrying a synthetic aperture radar (SAR). We use a stack of 13 scenes of the Northern Bohemia to assess the deformations in time in the area, particularly at some (coherent) parts of the scene: Most, Komořany and Louny sites. More data and more areas will be processed in future.

First, all possible interferograms are created from these scenes, the topography is subtracted and the interferograms are spatially filtered and unwrapped. Then, phase consistency for each pixel of the interferogram is checked and some pixels or interferograms are excluded from the following processing. Finally, adjustment is performed using two models: deformation and velocity models. Results not satisfying Kolmogorov-Smirnov test are excluded.

Contents

Chapter 1

Introduction

Synthetic aperture radar (SAR) interferometry (InSAR) processes a pair of satellite SAR images. The result may be a digital elevation model (DEM) or a map of Earth-crust deformations in the processed area.

The north-Bohemian coal basin is a largely unstable area. In addition to many huge open mines, it contains also deep mines, and some of them are very old and abandoned and may possess a potential danger for the people living in the area.

However, as a result of the previous ESA project, it is not reliable to estimate a deformation (or even its velocity) from one pair of SAR images, especially if the time between their acquisitions is rather short. On the other hand, if the time is long, the interferogram created from the images gets decorrelated due to many effects (most often the vegetation change) and the information gets lost.

The purpose of the ESA project nr. 3423 is to estimate the velocity of the subsidences in the area of north Bohemia using a stack of SAR images from different seasons within the 1996-2004 period.

Due to the fact that the processing is time and memory requiring, we do not process the whole scene, only specific areas (usually towns and cities). These areas were selected as coherent in an interferogram of about 13 months long temporal baseline. In some other interferograms, these areas are not coherent – these interferograms were excluded from the postprocessing. In addition, the urban areas are the most important to be monitored for subsidences.

The stack method involves processing of several interferograms with a common master, with respect to which the deformations are related. In order to achieve a larger number of interferograms, some of the slave scenes are resampled in order to correspond exactly (i.e. with subpixel accuracy) to the master. Then, any of these resampled scenes can be used as a master for creating other interferograms, although the baseline parameters etc. do not change by resampling.

The larger number of interferograms is not only usable in the case when some interferograms must be excluded due to a bad coherence (the bad coherence may be also crop-depending, i.e. different for different crops of the scene), but also for reducing errorneous influences in the deformation adjustment and for ambiguity resolution, which is an important part of the postprocessing.

In the InSAR method, all measurements are relative. In deformation mapping, a reference point (or area) must be said to be stable. The deformations can only be assessed with regard to a reference point. We do not know the areas in detail, and therefore are not able to determine the stable point; on the other hand, it may be decorrelated in some of the interferograms. That is why we select the stable point as the most coherent point in all interferograms. In this case, if an unstable point is selected, it looks stable but the surrounding, which really is stable, looks unstable.

However, for assessing the quality and reliability of the results, the knowledge of the area and a stable point is neccessary. A priori, we consider all points to be stable, and only those points, where the deformation standard deviation is much larger than the deformation itself, we may consider unstable. In future, we plan to perform geocoding of the interferograms and contact a person who knows the area in detail.

Another feature of the InSAR method is that the measured interferogram phase corresponds to the line-of-sight direction only. The deformation in the perpendicular direction cannot be assessed in any way.

On the other hand, if the deformations are computed independently from a stack of scenes acquired during descending passes of a satellite, and another stack is acquired during ascending passes of the satellite, the resulting 3D deformation may be computed if the scenes are geocoded properly.

Chapter 2

Data Used

track no.	satellite	date	perp. bas.
23428	ERS-1	1996-01-07	**0**
3755	ERS-2	1996-01-08	-69
24430	ERS-1	1996-03-17	77
4757	ERS-2	1996-03-18	100
25933	ERS-1	1996-06-30	6
9266	ERS-2	1997-01-27	26
10268	ERS-2	1997-04-07	254
15779	ERS-2	1998-04-27	91
16280	ERS-2	1998-06-01	155
40963	ERS-1	1999-05-16	107
28304	ERS-2	2000-09-18	130
29306	ERS-2	2000-11-27	171
31811	ERS-2	2001-05-21	81

Table 2.1: A part of the data used for the project. These data were already processed. Boldface denotes the master scene, with regard to which the perpendicular baselines are related.

The master of this stack is the image acquired from track **23428**. The following locations were processed: Louny (supposed to be stable), Komořany and Most (supposed to be unstable).

Out of the data listed in table 2.1, many interferograms were created for each of the selected location. In order to create interferograms with non-master images, all images are resampled with regard to the master scene. Then, all the resampled images do exactly correspond to the master scene.

However, not all of the interferograms were coherent. This may be caused by processing (inadequately estimated coregistration polynom between the two scenes), by acquisition in inappropriate season or by a long temporal baseline. These interferograms cannot be processed furthermore.

The topography was subtracted from the interferograms and the interferograms were filtered (using adaptive spectral filtering, `adf` script contained in the GAMMA software).

master	3755	23428	24430	4757	25933	9266	10268	15779	16280	40963	28304	29306	31811
3755	-	-	used	used	-	used	-	-	-	-	-	-	-
23428	used	-	used	used	used	-	-	used	used	used	used	used	-
24430	-	-	-	used	used	-	-	-	used	used	-	used	-
4757	-	-	-	-	-	-	-	-	-	-	-	-	-
25933	-	-	-	used	-	-	-	-	used	used	-	used	-
9266	-	-	-	-	-	-	-	-	used	-	-	-	-
10268	-	-	used	used	-	-	-	-	used	used	used	-	-
15779	-	-	used	used	used	-	-	-	used	used	used	used	-
16280	-	-	-	used	-	-	-	-	-	used	used	used	-
40963	-	-	-	used	-	-	-	-	-	-	used	used	-
28304	-	-	-	-	-	-	-	-	-	-	-	used	-
29306	-	-	-	used	-	-	-	-	-	-	-	-	-
31811	-	-	-	-	-	-	-	-	-	-	-	-	-

Table 2.2: Processed interferograms for the Louny location.

master	3755	23428	24430	4757	25933	9266	10268	15779	16280	40963	28304	29306	31811
3755	-	-	used	used	used	used	-	-	used	-	-	-	-
23428	used	-	used	used	used	-	-	used	-	-	used	used	-
24430	-	-	-	used	-	-	-	-	used	-	-	used	-
4757	-	-	-	-	-	-	-	-	-	-	-	-	-
25933	-	-	-	used	-	used	-	used	-	-	used	used	-
9266	-	-	-	used	-	-	-	-	-	used	used	-	-
10268	-	-	-	used	-	-	-	used	used	-	-	-	-
15779	-	-	-	-	-	-	-	-	-	used	-	used	-
16280	-	-	-	-	-	-	-	-	-	-	used	used	-
40963	-	-	-	-	-	-	-	-	-	-	used	used	-
28304	-	-	-	-	-	-	-	-	-	-	-	used	-
29306	-	-	-	-	-	-	-	-	-	-	-	-	-
31811	-	-	-	-	-	-	-	-	-	-	-	-	-

Table 2.3: Processed interferograms for the Komořany location.

master	3755	23428	24430	4757	25933	9266	10268	15779	16280	40963	28304	29306	31811
3755	-	-	used	used	-	-	-	-	-	-	-	-	-
23428	used	-	used	used	used	used	-	used	-	used	-	-	-
24430	-	-	-	used	used	used	-	used	-	used	used	used	-
4757	-	-	-	-	-	-	-	-	-	-	-	-	-
25933	-	-	-	used	-	used	-	used	used	used	used	used	-
9266	-	-	-	used	used	-	-	used	used	-	used	-	-
10268	-	-	-	used	-	-	-	used	-	used	used	used	-
15779	-	-	-	used	-	-	-	-	used	used	used	-	-
16280	-	-	-	used	-	-	-	used	-	used	used	used	-
40963	-	-	-	used	-	-	-	-	-	-	used	used	-
28304	-	-	-	used	-	-	-	-	-	-	-	used	-
29306	-	-	-	-	-	-	-	-	-	-	-	-	-
31811	-	-	-	-	-	-	-	-	-	-	-	-	-

Table 2.4: Processed interferograms for the Most location.

master	3755	23428	24430	4757	25933	9266	10268	15779	16280	40963	28304	29306
3755	0	72	148	172	77	97	326	160	228	170	204	242
23428	-72	0	79	105	6	27	254	90	160	98	131	173
24430	-148	-79	0	29	-73	-51	179	13	82	29	68	94
4757	-172	-105	-29	0	-100	-79	160	-23	56	-14	68	71
25933	-77	-6	73	100	0	22	250	85	155	93	127	167
9266	-97	-27	51	79	-22	0	229	63	134	73	108	146
10268	-326	-254	-179	-160	-250	-229	0	-167	-107	-156	-128	-91
15779	-160	-90	-13	23	-85	-63	167	0	71	18	57	83
16280	-228	-160	-82	-56	-155	-134	107	-71	0	-69	-70	17
40963	-170	-98	-29	14	-93	-73	156	-18	69	0	40	78
28304	-204	-131	-68	-68	-127	-108	128	-57	70	-40	0	70
29306	-242	-173	-94	-71	-167	-146	91	-83	-17	-78	-70	0

Table 2.5: Perpendicular baselines in meters for all pairs. The perpendicular baselines are computed with regard to the center of the scene. The table does not contain track 31811, which was used in no interferogram.

Chapter 3

Methodology

3.1 Interferogram creation

The first step of the processing is the interferogram creation. It consists of the following important steps:

- coregistration of the two scenes,
- resampling of the slave scene in order to correspond exactly to the master,
- subtraction of the slave phase from the master phase (interferogram creation),
- subtraction of the *flat-Earth* phase (i.e. the phase corresponding to the Earth surface without topography) from the interferogram. For the flat-Earth phase computation, orbital information is used.

3.2 Topography subtraction

A significant component of the phase information is influenced with topography. The coefficient of proportionality is influenced by the spatial baseline between the two scenes, particularly by the component perpendicular to the radar ray (perpendicular baseline).

There are two basic methods of topography subtraction:

- 2-pass method, i.e. using an external digital elevation model (DEM) as a topography information. Using orbital information, the DEM is converted into the radar system (i.e. a synthetic interferogram is created) and this is subtracted from the real interferogram. GAMMA software allows to create also a synthetic magnitude image to be coregistered with the magnitude image from the satellite; however, this possibility was not used for the processed scene crops. The synthetic magnitude image is created from the DEM information only and therefore does not contain man-made features, which are most significant in the satellite magnitude image. Due to this fact the coregistration of the small scene crops fails. However, as proven in the whole scene processing, the orbits are in most cases precise enough such that the difference between the synthetic and real magnitude is not higher than one pixel. We use the SRTM (Shuttle Radar Topography Mission) DEM, which is created by InSAR method, and therefore some properties may be similar.
- 3-pass method, i.e. using a different interferogram for topography subtraction. The phase of this interferogram must be unwrapped which may be a problem in incoherent areas. We decided not to use this method in the project.

3.3 Coherence and filtering

For coherence computation, the coregistered scenes (slave scene resampled) are used. The coherence is (according to [5])

$$\gamma_c = \frac{\frac{1}{N}\sum_{i=0}^{N} M \cdot S^*}{\sqrt{\frac{1}{N}\sum_{i=0}^{N} M \cdot M^* \frac{1}{N}\sum_{i=0}^{N} S \cdot S^*}}, \tag{3.1}$$

where M, S are the complex value of a pixel in the master and slave images and N stands for the size of a window used for coherence computation. Unfortunately, the coherence estimation is biased for small windows and small coherence values (see e.g. [5]); however, at the time there is no other possibility to estimate the value better. Large estimation windows may cause coherent areas to get lost.

The coherence is related to the phase standard deviation with the following equation:

$$\sigma_{\Delta\varphi} = \frac{1}{\sqrt{2N}} \frac{\sqrt{1-\gamma^2}}{\gamma} \tag{3.2}$$

where $\gamma = |\gamma_c|$ is the real coherence and N is the number of samples multilooked to one interferogram pixel. (For our interferograms, $N = 9$.) However, this equation only holds for point scatterers [5], for gaussian scatterers the probability density function is much more complicated.

Although the condition of point scatterers is not generally satisfied, phase standard deviations for each pixel in each interferogram in the stack are used for weight computation during adjustment and for statistical tests.

After topography subtraction, the phase of the interferogram is filtered using the adaptive algorithm implemented in the GAMMA software (`adf` script). Filtering is performed on the basis of a local fringe frequency, in order not to filter out the high-frequency component of the phase (which is usually not neccessary if filtering topography-subtracted interferogram). More details about the algorithm may be found in [2].

3.4 Phase unwrapping

The actual phase value is by definition in the $(-\pi, \pi)$ interval, therefore is ambigous. Phase unwrapping is a process of finding ambiguities k so that $\varphi + 2k\pi$ is the real (unwrapped) phase.

However, it is not possible to recover the real phase from the wrapped one. First, the absolute ambiguity k to be added to the whole interferogram must be known. This can be easily solved by selecting a reference point, for which the ambiguity is zero. Due to the fact that all measurements are relative, the selection is arbitrary.

In order to make the phase unwrapping unambiguous at least in ideal cases, the assumption of spatial phase continuity is adapted. It means that the phase difference between two neighbouring pixels is in the $(-\pi, \pi)$ interval. In our case the assumption is helped by the fact that the interferogram contains only deformation signal (and noise).

If the assumption is fulfilled, the phase unwrapping is a trivial task: all phase differences are preserved and the ambiguitites are found using the ambiguities of the neighbouring pixels.

The points, where the assumption is not fulfilled, can be easily found out and are called residues. Between individual residues, *branch cuts* are created and the unwrapping paths are not allowed to cross them. Branch cuts creation is an ambiguous problem and its solution is not trivial. Several methods are applied for this problem, some of them even use a different information, such as weights (coherence), scene magnitude (possible layover effects, when unwrapping topography data) etc.

When the area to be unwrapped contains low-coherent regions, which causes the rest of the area to break up into separated regions, only one of this regions is unwrapped (the one that contains the reference point, at which the unwrapping starts).

Although the phase in an interferogram with subtracted topography does not exceed one phase cycle, the interferogram must be unwrapped. In the case of not-unwrapped interferogram, the problem would be at the points where the phase changes its sign – the phase would not be continuous here, causing errors in postprocessing.

Phase unwrapping can be performed as a part of interferometric processing in the GAMMA software.

3.5 Data byteswap

The GAMMA software, although compiled from sources on a little-endian computer, works in a big-endian representation. Therefore, the interferograms and coherence maps must be byteswapped before importing to another software working in little endian, such as MATLAB.

Similarly, all external data to be used within computations in GAMMA, must be in big endian. The DEM for topography subtraction, exported from GRASS for little-endian platform, must be byteswapped. However, the SLC data are provided by ESA in the big-endian representation.

3.6 Interferograms related to one reference point

As already noted in the introduction, the interferogram phase is only a spatially relative information. That means a point in the interferogram must be considered to be stable, and the deformation of the other points are related to this one.

However, the selection of the reference point is not as crucial as it may seem. If the point is unstable (and subsiding), the really stable points seem to be uplifted. We do not expect any uplifts in the area of interest.

The phase value of the reference point must be known for all interferograms. In the case that there is no point for which phase values are known in all interferograms, a point must be selected and that interferogram, for which the phase information is not known (due to e.g. phase unwrapping), must be excluded from the postprocessing.

As a reference point, the most coherent point from all interferograms, i.e. a point satisfying maximum in

$$\sum_{k=1}^{k=s} \gamma(i,j,k)^2 \tag{3.3}$$

was selected. Here, s is the number of interferograms and γ is the coherence value of the pixel i, j in the interferogram k.

Now, the phase values of each interferogram must be reduced be the phase value of the reference point. In order for the resulting phase values to be in the $(-\pi, \pi)$ interval, the reduction is not performed by phase subtraction, but by complex conjugate multiplication.

3.7 Interferogram consistency check

According to [6], the phase of three interferograms φ_{AB}, φ_{CA} and φ_{BC}, created from three scenes A, B, C must satisfy the following condition:

$$\varphi_{AB} + \varphi_{CA} + \varphi_{BC} = 0, \tag{3.4}$$

the signs may be altered with respect to the sequence of master and slave.

As verified in the case of a randomly selected three interferograms, this condition is approximately fulfilled for most of the pixels.

We can now distinguish two cases of not-fulfilling this condition:

- the sum is (at least approximately) $2k\pi$, in this case one or more of the phases must be shifted by $2l\pi$, where both k, l are integers,
- the sum has a different value, this case cannot be resolved without changing on of the values, and may be caused by two influences:
  - the coregistration of the three interferograms was performed independently, i.e. there may be small coregistration errors,
  - the phase was filtered, and the phase value may change significantly in decorrelated areas; in this case, the phase quality is so low that it cannot enter the final deformation adjustment.

The process of consistency check has three steps:

1. Construction of interferogram triples. All interferogram triples are selected and then tested, if they cover only three scenes and are therefore to be summed to 0. In fact, also longer graph cycles may be selected, but this task is too time requiring due to the number of arcs (interferogram) – between 30 and 50. In the future, tetragons may be implemented too, if the number of triangles is found not to be sufficient.

   A matrix C is constructed in this step: the number of columns corresponds to the number of interferograms, and the number of lines corresponds to the number of cycles. Each line contains three non-zero elements: 1 means that the phase of the interferograms must be added, -1 means that the phase must be subtracted in order to give 0.

2. Check for the coregistration/filtering errors. In this step, the phases are not summed up, but complex numbers with a unique amplitude are constructed and multiplied (in the case of a negative sign, the complex number is conjugated before multiplication). The interferograms in triples, in which the product phase is near zero, are considered to be all OK. The tolerance is set to $\pm 2\sqrt{3}\frac{2\pi}{10}$, considering the phase standard deviation to be $\frac{\pi}{10}$, although the interferogram phases are not independent.

   Some interferogram triples are considered bad. If two of the three interferograms are OK, the "corrected" phase of the third is computed from the other two. This corrected phase is then used to assess the quality of the other interferograms; however, it does not enter the final deformation adjustment.

   The advantage of the complex (conjugate) multiplication is evident: the resulting phase is in the $(-\pi, \pi)$ interval, and therefore all sums with an inappropriate ambiguitites (although OK) sum up to 0.

3. Ambiguity resolution. We only process the interferograms evaluated to be OK in the last step. The phase sums r for all interferogram triples are computed, divided by 2π and rounded in order to give integers. Now, the equation may be constructed:

   $$C \cdot x = r, \tag{3.5}$$

   where x is the vector of ambiguities k for each interferogram. However, the C matrix is singular and an integer solution is required.

   The Singular Value Decomposition (SVD) technique allows to resolve a similar problem with C singular, but it does not give the integer solution. The additional condition of the SVD technique is that the solution fulfills the minimum norm condition for the x vector, which is in accord with the interferometry requirements.

   The problem of ambiguity resolution is not uniformly solved in the interferometric literature. We decided to compute the SVD solution iteratively: each time the interferogram phase with the (absolutely) largest value of x is shifted by 2π in the appropriate direction and the absolute sum of the r vector is lowered. In all cases, a solution is found. This solution may not fulfill the minimum norm condition, which is not a problem in interferometry – however, the problem may have more minimum-norm integer solutions which may be equivalent with regard to mathematics, but not with regard to the reality.

However, this solution is not robust – in a case of a small change in the r vector, significantly different ambiguity vector is computed.

The interferogram triples are computed just once for each location (and the corresponding interferograms). However, the steps 2 and 3 are performed independently for each pixel. Although computationally requiring, the computation takes a reasonable time in MATLAB for small interferograms (approx. 200 by 200 pixels).

A significant disadvantage of performing the computations independently for each pixel is that the computed ambiguities may not be smooth spatially, causing the unwrapped phases to be nonsenseful. Therefore, we decided to use the same ambiguity vector for all pixels – that one which was computed for most of the pixels. Due to the fact that all interferograms are unwrapped, it is reasonable to apply a single ambiguity to the whole interferogram.

3.8 Adjustment model

The interferometric phase (after topography subtraction) contains the following components:

- DEM errors (this component is directly propotional to the perpendicular baseline),
- deformation signal (possibly split into linear and nonlinear components),
- atmospheric delay (i.e. the difference between the delay in the master and slave scenes),
- noise.

In the literature dealing with interferometric stacks, there are basically two models for deformation adjustments:

- *deformation model*, where the deformations in the times of acquisitions are searched for,
- *velocity model*, where the deformations are considered linear in time and their velocity is searched for, together with other parameters.

Both approaches have their advantages and disadvantages, which will be discussed below.

For both approaches, let us introduce the following vectors and matrices:

- matrix A denoting which interferogram was created from which scenes: it has n columns (one for each scene) and m rows (one for each interferogram) and contains -1 if the corresponding scene was master for the interferogram, and 1 if it was slave.
- vector of acquisition times t, containing n rows, one for each scene. Due to the fact that the ERS-1/2 satellites are sunsynchronous and moving on the same orbit, the time of day of all the acquisition times is the same. Therefore, the values in t are integer multiples of days.
- vector of temporal baselines dt, containing m rows, one for each interferogram. Here, $dt = A \cdot t$.
- vector of perpendicular baselines B, containing m rows, one for each interferogram. The perpendicular baselines is used for assessing the DEM error and do not need to be precise. Although the perpendicular baseline significantly changes within an interferogram, the values computed for the scene center (i.e. the values are the same for all locations) are used. The ratio between the used and true baseline should be almost the same for all interferograms in a stack. The GAMMA software does not provide the perpendicular baseline length, so the baselines were computed in the DORIS software.
- vector of the measured phases φ, containing m rows, one for each interferogram.

Let us note here that both models assume that the adjustment is performed independently for each pixel of the interferogram stack.

3.8.1 Deformation model

This deformation model is described and applied in [6].

Before the processing itself, matrix A needs to be regularized, which may be performed by eliminating the column corresponding to the master scene, in which acquisition time the deformations are considered to be zero.

Then,

$$A \cdot \Phi = \varphi + \delta\varphi, \tag{3.6}$$

where Φ is the vector of adjusted deformation in the time of acquisition of each interferogram and $\delta\varphi$ is the phase noise to be minimized in the least-squares adjustment.

Let us note here that this deformation model does not need any assumptions of the deformation linearity in time. However, it does not assess DEM errors. Atmospheric influence is said to be partially eliminated in the adjustment.

Due to a large number of unknows, there may be a problem of the regularity of the matrix $A^T A$. During the interferogram consistency check steps, some interferograms may be excluded from the adjustment, causing that some columns of the A matrix may be empty or there are more independent sets of scenes, which are not interconnected by any interferogram. In both of these cases, the matrix $A^T A$ is singular and there are two ways of solving it:

- excluding the empty columns from the matrix A, eventually separating the independent sets of interferograms into more matrices and adjusting independently; however, some elements of the vector Φ are missing in the case of exclusion and the independent sets of vector Φ, computed by separate adjustment, may not be interconnected in any way without a priori information (e.g. from neighbouring pixels or by temporal interpolation).

- using the already noted SVD technique. However, this method has some disadvantages: it provides no weighted solution, so no weights can be introduced into the adjustment. The other disadvantage is that the results may not correspond to the physical reality, as noted in [1], where the SVD technique with the velocity model is recommended.

3.8.2 Velocity model

The velocity model, described and applied in [1], assumes that the deformations are linear in time, respectively the deformations may be represented by an explicit function of which the parameters are searched for.

The linear velocity model can be expressed in the following way:

$$\varphi = \frac{4\pi}{\lambda} dt \cdot v + \frac{4\pi}{\lambda} \frac{B}{r \sin\Theta} \cdot \Delta z + \delta\varphi, \tag{3.7}$$

where v is the deformation velocity, r is the slant range and Θ is the look angle. Δz is the DEM error, which does not depend on the temporal baseline dt, but on the perpendicular baseline B, and $\delta\varphi$ is again the phase noise to be minimized by the least-squares adjustment.

A great advantage of this model is that the number of unknowns is small and therefore there are no problems with singularity. However, the problem is that the parametric expression of the deformations may not be known in advance and that the assumption of linearity may not be always satisfied.

3.9 Quality and reliability of the results

The accuracy of the results (i.e. deformations at the times of acquistion, resp. deformation speed) depends on many factors. First, let us mention the random phase noise, which also influenced the previous processing and caused some interferograms to be excluded from the adjustment.

A priori, we consider the area (all pixels of the interferograms) to be stable. The null hypothesis of the stability may be disclaimed with some criteria. The first way suggested is to filter out the deformations which are smaller than a multiple of their standard deviation.

However, this approach cannot be used in our case due to the fact that we do not know if our reference point is really stable.

Due to the fact, we decided only to eliminate the results which are not reliable, i.e. their standard deviation is too high or we reject the hypothesis of the reliability of the adjustment model with respect to statistical tests.

We tried three ways to filter out the irreliable results:

- A threshold for the deformation standard deviation was suggested and points, whose deformation standard deviation was larger, were considered irreliable.
- As suggested in [6], the adjustment residues were tested if they are normally distributed with the a priori precision. The a posteriori standard deviation and the a priori standard deviation are compared and tested. Here, only the standard deviation is tested, not the normality.
- The residues are tested for normality using the Kolmogorov-Smirnov test, as implemented in MATLAB in the `kstest` command. Here, the values of $\frac{s}{\sigma_{\Delta\varphi}}$, where s are the residues for one pixel and $\sigma_{\Delta\varphi}$ is the a priori standard deviation (computed from the coherence using expression (3.2)), are tested to be normally distributed with zero mean and unique standard deviation.

3.9.1 Snedecorov-Fischer distribution

In accord with [3], let us have two independent variables y_1 and y_2 with distributions $\chi^2(n_1)$ and $\chi^2(n_2)$, where n_1 and n_2 are degrees of freedom of the respective distributions.

Their ratio

$$F = \frac{\frac{y_1}{n_1}}{\frac{y_2}{n_2}}, \tag{3.8}$$

has then Snedecorov-Fischer distribution $F(n_1, n_2)$.

We need to compare the a priori and a posteriori standard deviations. Here, in order to set the same value for all of the a priori phase standard deviation, we use the value of $\sigma_{\Delta\varphi} = \frac{2}{10}\pi$, while the a posteriori phase standard deviation can be computed from the adjustment residues.

Let us now consider the phase residues are normally distributed with zero mean. We then substitute

$$\frac{y_2}{n_2} = \sigma^2_{\Delta\varphi}, \tag{3.9}$$

with $n_2 = \infty$, and

$$y_1 = s^T P s, \tag{3.10}$$

where s are the adjustment residues and P is the weight matrix. Here, n_2 is the number of redundant interferograms, i.e. the number of interferograms (after exclusion) minus rank $A^T PA$ (for the case of deformation model) or minus 2 (for the case of the velocity model).

The value F is then compared to $F_\alpha(n_1, n_2)$, known from the Snedecorov-Fischer distribution, and if $F > F_\alpha$, then the hypothesis of a reliable result is rejected with the confidence level α.

Numerically, MATLAB is unable to compute a reasonable value of F_α for $n_2 = \infty$. In our case (low values of n_1), we can substitute it by $n_2 = 1000$ (the value then differs at the third decimal position).

3.9.2 Kolmogorov-Smirnov test

The Kolmogorov-Smirnov test allows to test if a data set belongs to a certain distribution. In our case, we test if the data set of $\frac{s}{\sigma_i}$ has the normal distribution N(0,1). In comparison to the Fischer test described above, this one does not only test the standard deviation, but also the normality of the residues. This test is described in detail in MATLAB help.

3.10 Geocoding

In the topography subtraction step, the lookup table converting map to SAR coordinates, was created. As already noted, GAMMA allows to coregister the DEM with the SAR magnitude, but this process was not successful in our case – the areas are too small and artificial objects are more clear in the magnitude image. However, trying to geocode the whole scene, we found out that the difference between the DEM and interferogram is few pixels. We therefore consider geocoding to be precise enough.

The last step is the conversion of the computed velocity maps into map coordinates. It is performed with regard to the DEM processed in the topography subtraction step, and therefore the coordinates are in the same system, i.e. WGS-84. In GAMMA, the script to perform the conversion is called `geocode_back`.

3.11 Problems

3.11.1 Atmosphere

The phase of the signal received by radar is influenced by refractive index n – the speed of light in the atmosphere is not exactly c. In SAR literature (see e.g. [4]), the atmospheric delay is usually said to originate in

- ionosphere, where the delay is caused by a different concentration of free electrons – the concentration is dependent on "solar activity, time of day, latitude and geomagnetic activity." Of these, latitude and time of day is the same for each pass and the other parameters do not change quickly within the imaged area, and therefore should cause only low-pass effects.
- troposphere, where the delay is caused by variations in "temperature, pressure and relative humidity." Most of the delay variations are also large-scale in comparison to our processed crops. An atmospheric delay ramp may be caused by a frontal zone [4] or convective cells. A frontal zone may be easily found in meteorological data; however, there is not much known about the convective cells. On the other hand, the phase in our data is usually quite stable.

3.11.2 Orbit errors

As already noted, the orbit errors are usually small enough not to influence the adjustment. The residual fringes do not appear in the small processed areas, if Delft precise orbits are used in processing. However, the Delft precise orbits (or at least fast-delivery orbits, which are only available for some periods of time) are not available for all scenes. The very late ERS-1 scenes have only the current orbits available, which are the part of the received data. The precision of these data is said to be in the order of meters, which is obviously too much, because all interferograms where one of these scenes is used, contain residual fringes.

The GAMMA software allows to compute the baseline from the fringe frequency and subtract the flat-Earth phase according to it, but this process was successful only for a part of the scenes, and therefore we did not use it at all. The residual fringes were corrected by the `cpxdetrend` script, which only allows to subtract the linear component of the residual phase.

Chapter 4

Results and Conclusion

In figures 4.1, 4.3, 4.5, the deformation velocities of the processed locations are displayed. Figures 4.2, 4.4, 4.6 show the deformations between the first and last interferferograms of the processed set. Velocities are evaluated in mm/yr, deformatins in mm. The colorscale is displayed in figure 4.7.

The Komořany site needs to be processed in two separate regions, because of an error in the DEM which causes the topography-subtracted interferograms to contain inappropriate values in a line throughout the area. Therefore, the upper and lower parts of the area are presented separately. Please note that in table 4.1, the total number of pixels is referred to the whole area.

However, we did not unwrap each individual region. Mostly, some regions got separated in the interferograms with lower coherence, not in all interferograms. Processing all the regions would mean processing them independently. In the cases where just a part of a region was able to be unwrapped, we selected the largest and the most important part.

The non-unwrapped regions of the interferograms did not enter the adjustment, i.e. the number of interferograms varies significantly throughout the area. Due to the fact that no pixel was unwrapped in all areas, whole interferograms had to be excluded in order to select a reference point.

Table 4.1 lists the numbers of valid pixels for each location and model. Due to a very small numbers of valid pixels for the Snedecorov-Fischer test, only the Kolmogorov-Smirnov test filtering is applied for display and further analysis.

site	pixels total	valid pix. – velocity model		valid pix. – def. model	
		K-S test	S-F test	K-S test	S-F test
Komořany – upper	29.659	2.734	22	5.092	356
Komořany – lower	29.659	3.137	26	5.878	507
Louny	70.645	5.335 (8 %)	15 (0 %)	29.065 (41 %)	458 (1 %)
Most	48.930	3.599 (7 %)	1 (0 %)	16.971 (35 %)	153 (0 %)

Table 4.1: The number of valid pixels (i.e. pixels passing the Kolmogorov-Smirnov (K-S) test or Snedecorov-Fischer (S-F) test) for each location and model

4.1 Discussion

There is a difference between the results of the deformation and the velocity models. The deformation model results do not look very smooth, although the interferograms are smooth. However, the number of valid pixels is much larger for the deformation model than for the velocity model, for both statistical tests. We attribute this difference to the generality of the model (i.e. that the velocity model assumes the deformations to be linear in time) and to the number of redundant measurements (it is much smaller in the case of the deformation model, i.e. larger residues are allowed).

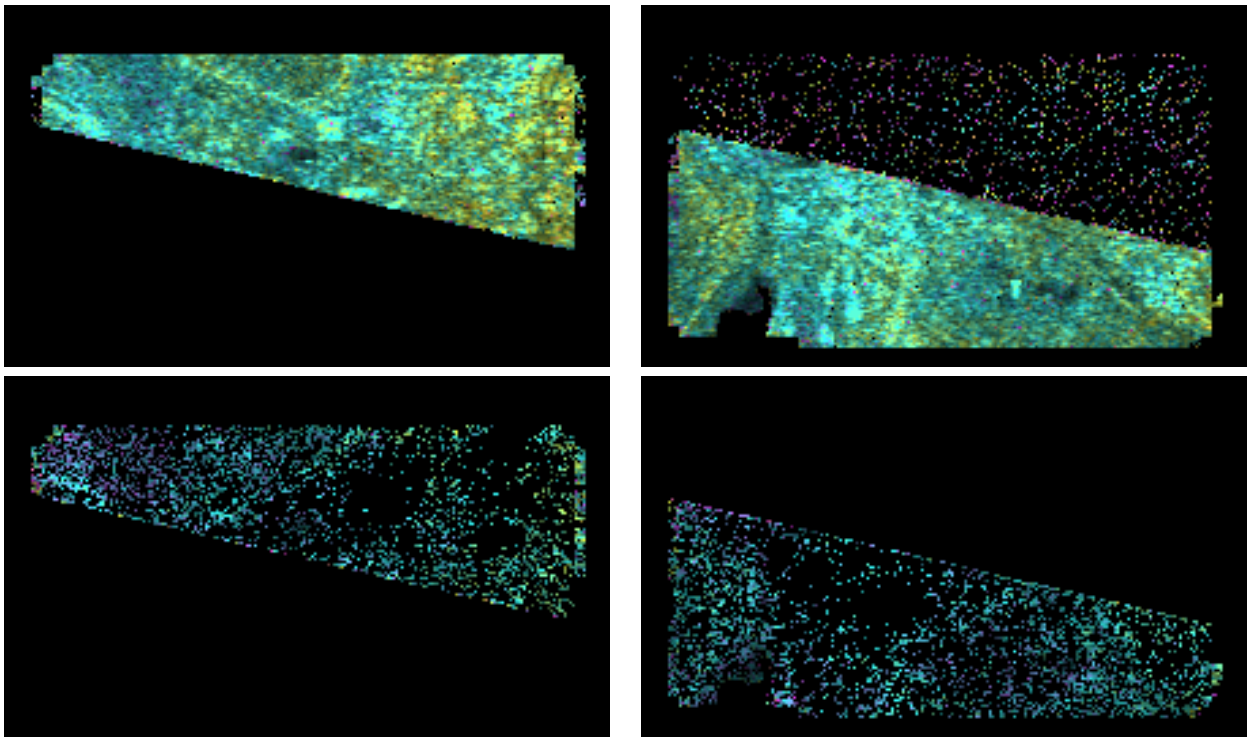

Figure 4.1: The deformation velocities at the Komořany site. In the upper part of the figure, all points are displayed, the points for which $\sigma_v > 5mm/yr$, are assumed to be stable. The reference point for the upper part is (line, pixel): 47, 138, for the lower part: 86, 85, the colorscale is displayed in figure 4.7. In the lower part of the figure, points which did not pass the Kolmogorov-Smirnov test, are displayed in black.

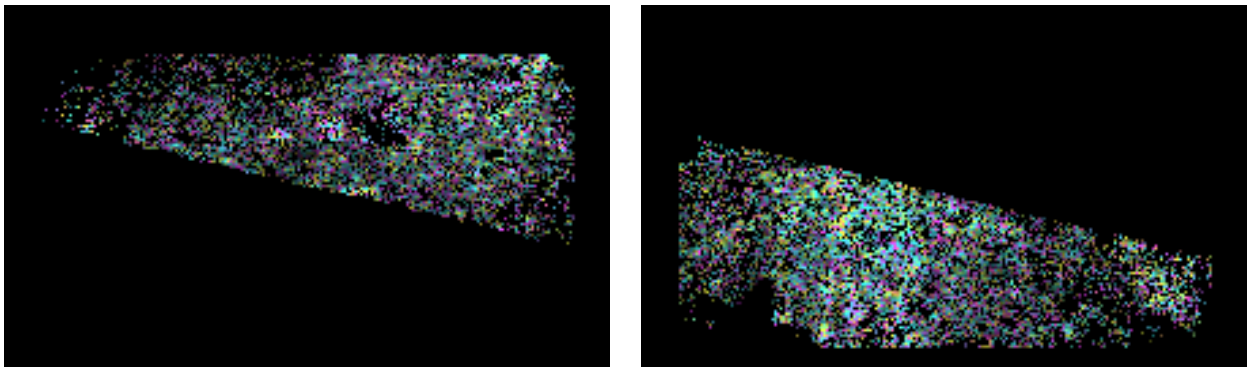

Figure 4.2: The deformations between January 1996 and November 2000 at the Komořany site. The points, which did not pass the Kolmogorov-Smirnov test, are displayed in black. The reference point for the upper part is (line, pixel): 47, 138, for the lower part: 86, 85, the colorscale is displayed in figure 4.7.

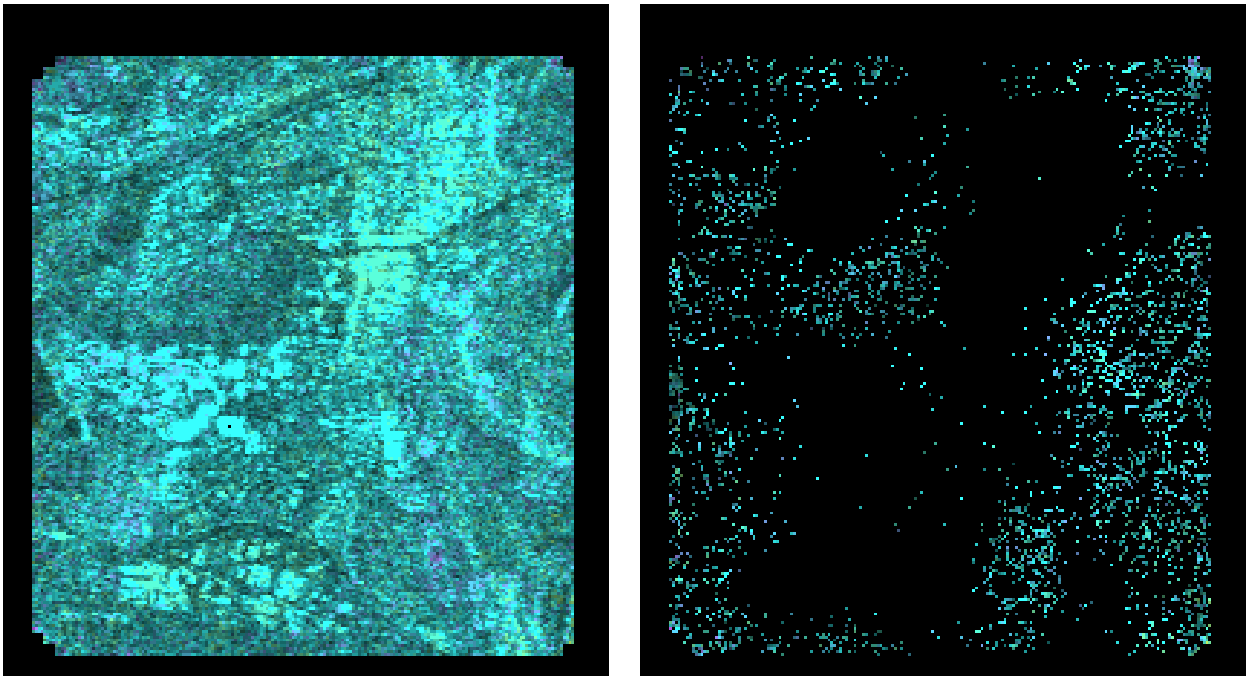

Figure 4.3: The deformation velocities at the Most site. In the left image, all points are displayed, the points for which $\sigma_v > 5mm/yr$, are assumed to be stable. In the right image, the points, which did not pass the Kolmogorov-Smirnov test, are displayed in black. The reference point is (line, pixel): 147, 79, the colorscale is displayed in figure 4.7.

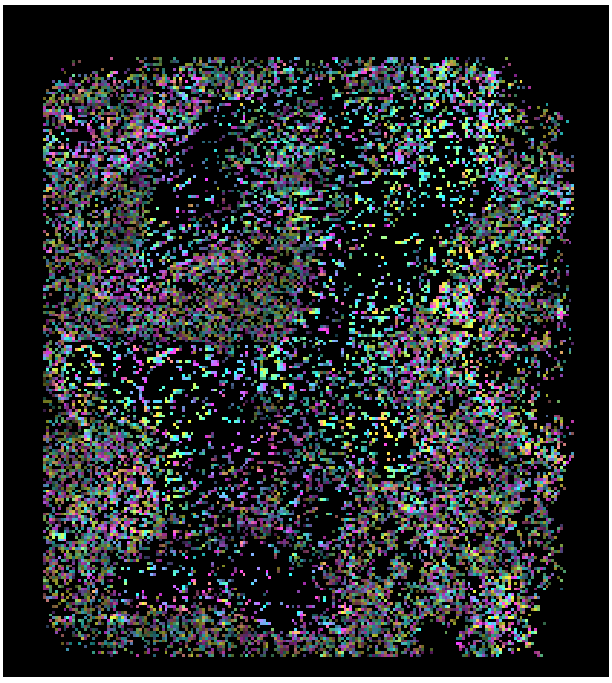

Figure 4.4: The deformations between January 1996 and November 2000 at the Most site. The points, which did not pass the Kolmogorov-Smirnov test, are displayed in black. The reference point is (line, pixel): 147, 79, the colorscale is displayed in figure 4.7.

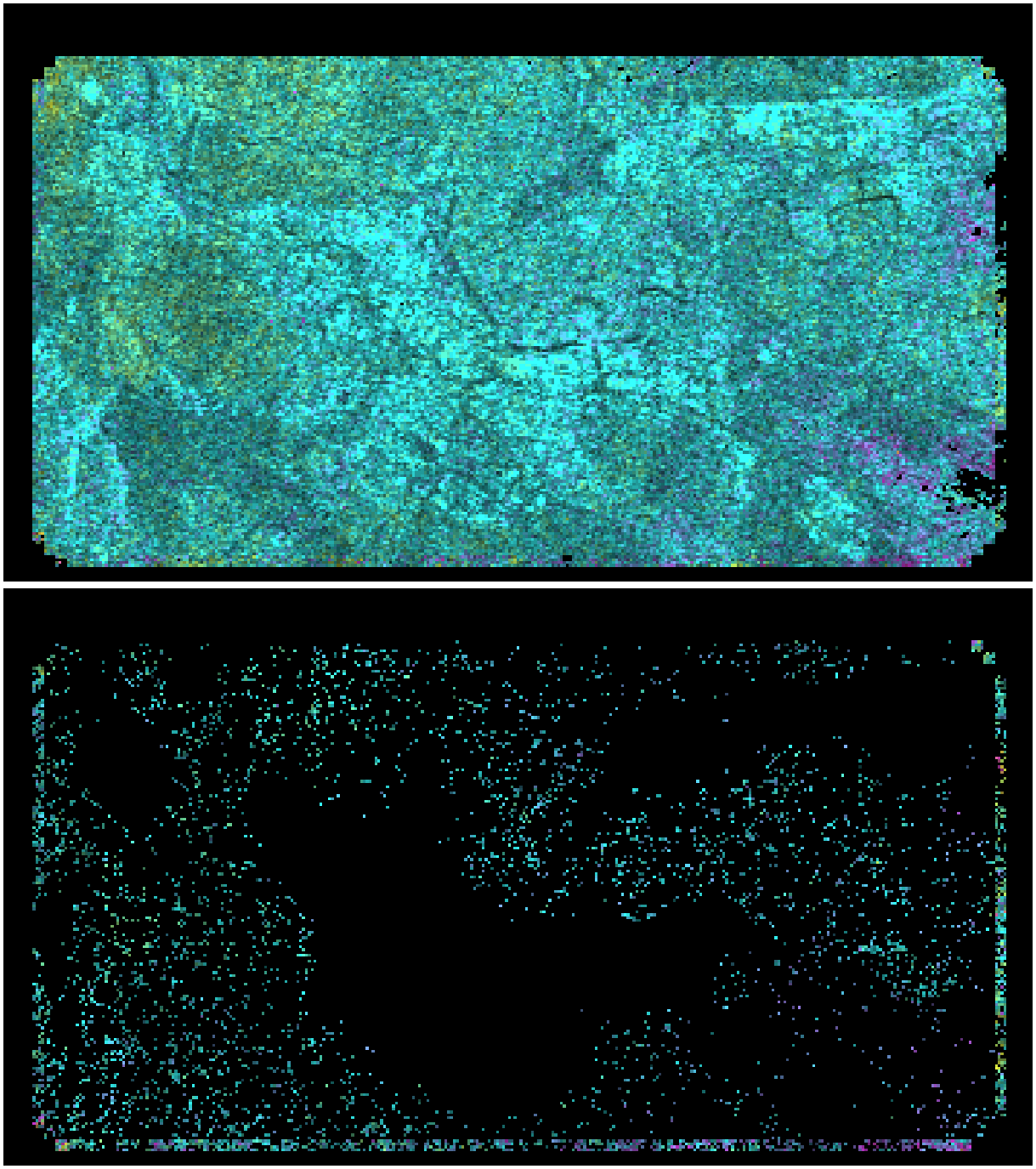

Figure 4.5: The deformation velocities at the Louny site. In the upper image, all poins are displayed, the points for which $\sigma_v > 5mm/yr$, are assumed to be stable. In the lower image, the points which did not pass the Kolmogorov-Smirnov test, are displayed in black. The reference point is (line, pixel): 104, 138, the colorscale is displayed in figure 4.7.

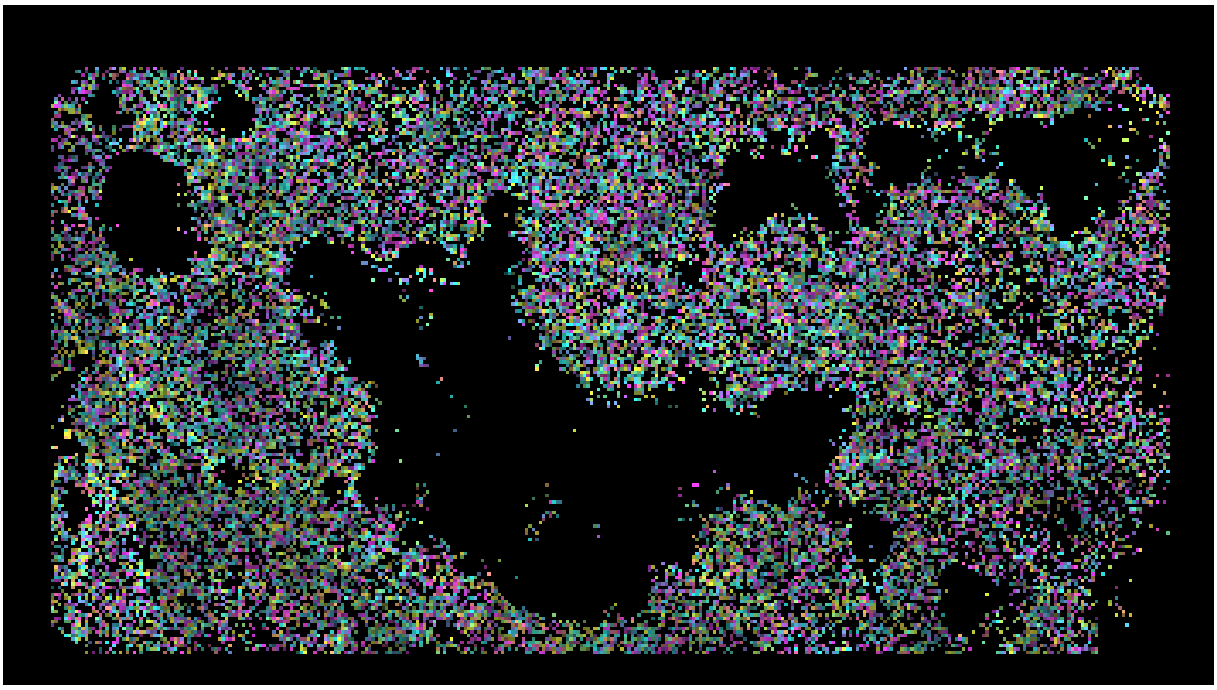

Figure 4.6: The deformations between January 1996 and November 2000 at the Louny site. The points, which did not pass the Kolmogorov-Smirnov test, are displayed in black. The reference point is (line, pixel): 104, 138, the colorscale is displayed in figure 4.7.

a b

Figure 4.7: Color scales for the deformation maps (a) or coherence maps (b). For deformation mapping, deformations are evaluated in mm, for velocity mapping, velocities are evaluated in mm/yr.

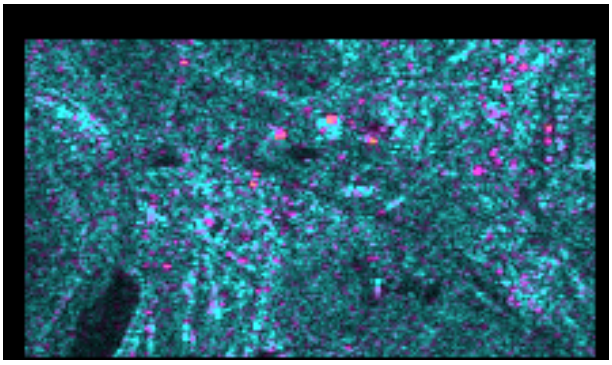

Figure 4.8: The coherence map of the upper part of the Komořany site, taken for the image pair 23428 (January 1996) and 28304 (September 1999). The coherence scale is displayed in figure 4.7. Image intensity corresponds to the scene magnitude.

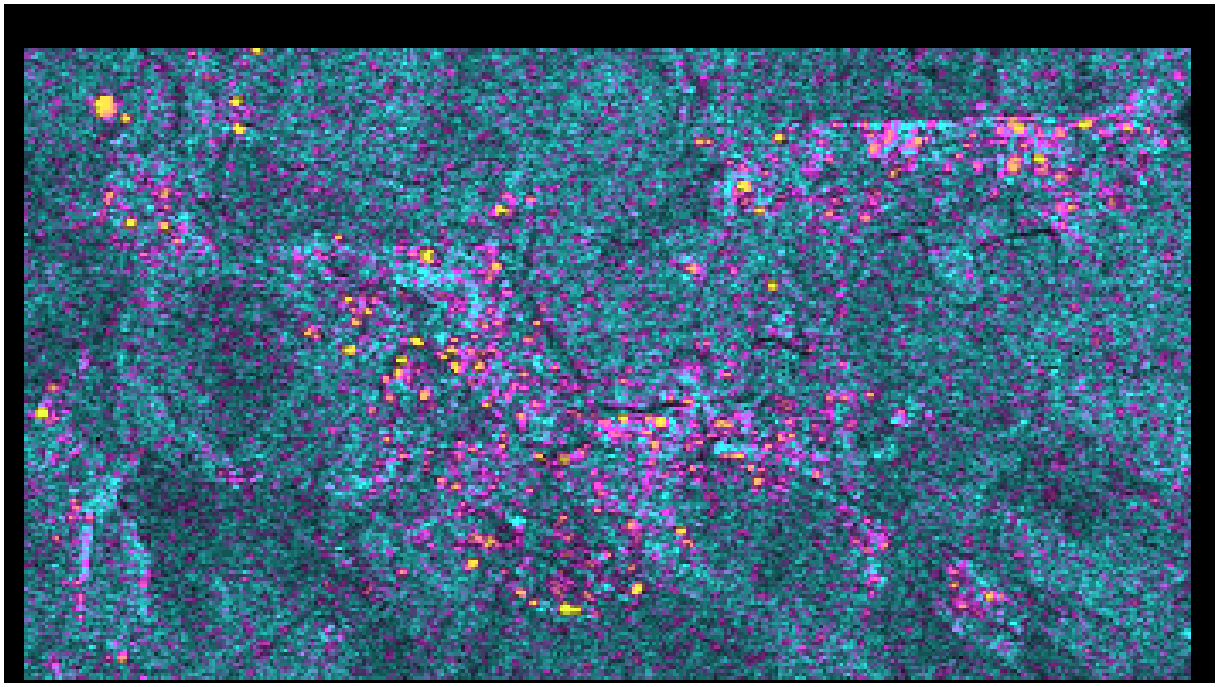

Figure 4.9: The coherence map of the Louny site, taken for the image pair 23428 (January 1996) and 40963 (May 1999). The coherence scale is displayed in figure 4.7. Image intensity corresponds to the scene magnitude.

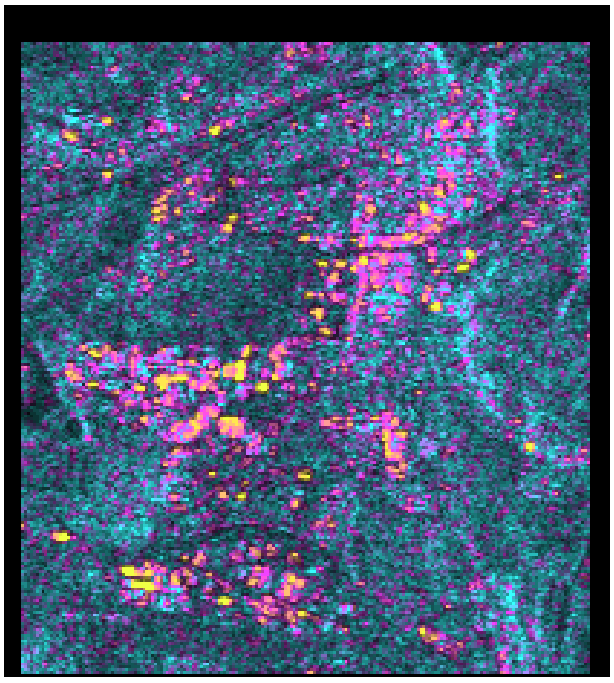

Figure 4.10: The coherence map of the Most site, taken for the image pair 23428 (January 1996) and 40963 (May 1999). The coherence scale is displayed in figure 4.7. Image intensity corresponds to the scene magnitude.

site	max. velocity	σ	point (l,p)	min. velocity	σ	point (l,p)
Komořany – upper	28	24	31, 14	-17.0	2.3	41, 14
Komořany – lower	40	28	47, 12	-57	32	115, 211
Louny	20.2	4.0	194, 19	-30	14	194, 20
Most	4.3	1.2	217, 11	-4.3	1.6	222, 197

site	max. velocity	σ_v	point (l,p)	min. velocity	σ_v	point (l,p)
Komořany – upper	23.8	1.5	34, 14	-17.0	2.3	41, 14
Komořany – lower	25.24	0.12	118, 212	-24.0	1.1	49, 11
Louny	20.2	4.0	194, 19	-29.9	4.2	193, 20
Most	4.3	1.2	217, 11	-4.3	1.6	222, 197

Table 4.2: Maximum velocities in each locality and their standard deviations. The points which do not satisfy the Kolmogorov-Smirnov test, are excluded. The upper table values are maximized over all pixels; in the lower table, pixels with $\sigma_v > 5mm/yr$ are assumed to be stable. All values are in mm/yr.

site	max. deformation	point (l,p)	min. deformation	point (l,p)
Komořany – upper	21	39, 117	-22	203, 31
Komořany – lower	23	62, 18	18	107, 126
Louny	20	121, 311	-22	63, 137
Most	28	176, 30	-24	21, 69

Table 4.3: Deformation between January 1996 and November 2000 at all sites. The points which do not satisfy the Kolmogorov-Smirnov test, are excluded. All values are in mm. Standard deviations are not included due to a relatively small number of redundant measurements.

We expect the deformations to be spatially smooth, so we do not consider the deformation model to give good results. However, the velocity model results do not show deformations at all, though they are expected at the Komořany and Most sites.

The large difference between the numbers of valid pixels for both statistical tests can be explained by the fact that different a priori standard deviation are accounted for. In the case of the Snedecorov-Fischer test, one a priori standard deviation is assumed for all interferograms in the set, independent of their coherence. However, thresholding of the applied interferograms in that sense that interferograms with smaller coherence than 0.3 were excluded from adjustment, helped to increase the number of valid pixels only negligibly.

On the other hand, the a priori phase standard deviations for the Kolmogorov-Smirnov test are computed separately for each interferogram, as a function of coherence, using formula (3.2). However, the phase standard deviation is underestimated for non-point target scatterers, mostly scatterers with a wrong coherence.

The Komořany site has many more valid pixels than the other sites (percentually). We attribute it to the smaller amount of interferograms, i.e. smaller number of degrees of freedom and therefore larger allowed residues.

The velocity maps which contain all pixels, not only the ones that satisfy the Kolmogorov-Smirnov test, do show some unstable areas, see e.g. the Louny site in figure 4.5. However, as seen in figure 4.14, the larger deformations are not spatially smooth and their standard deviation is also large.

The spatial non-smoothness of the deformation velocities suggests to filter the results before further analysis using a low-pass filter; however, the interferograms were already filtered in order to be unwrapped.

Certainly, some testing is neccessary in order to eliminate results originating from badly-scaled matrices which originate from an insufficient number of measurements for a pixel: most measurements were excluded due to inconsistency with the others or due to not being unwrapped.

In addition, the low number of valid pixels with regard to the Kolmogorov-Smirnov test may be caused

Komořany	latitude [deg]	longitude [deg]	Y[m]	X[m]
north	50.53786	13.54033	797793	984508
west	50.52036	13.53242	798636	986350
south	50.51245	13.58700	794937	987793
east	50.52828	13.59450	794152	986129
reference - upper part	50.518910	13.557258	796918	986770
reference - lower part	50.521305	13.569854	795995	986639

Most	latitude [deg]	longitude [deg]	Y[m]	X[m]
north	50.52036	13.62367	792236	987304
west	50.48536	13.61013	793758	991014
south	50.47724	13.66096	790322	992437
east	50.51161	13.67659	788666	988817
reference	50.493279	13.648156	790960	990539

Louny	latitude [deg]	longitude [deg]	Y[m]	X[m]
north	50.38224	13.76117	784818	1003928
west	50.35432	13.74846	786164	1006869
south	50.33786	13.84388	779709	1009663
east	50.36786	13.85805	778231	1006506
reference	50.358469	13.815148	781402	1007100

Table 4.4: Approximate corners of the scene crops for all sites. Latitude and longitude refer to the WGS-84 system, Y and X refer to the S-JTSK system.

by the fact that the velocity is not constant in time, but the deformations really occur. (However, the results of the deformation model do not correspond to this possibility). Different parametric models may be applied here, reducing the number of redundant measurements. Also, an a priori information about the deformation velocity should be known to design the model.

We consider the following filtering method to be the best in future: all pixels, for which the deformation velocity is smaller than a multiply of its standard deviation, are assumed to be stable. However, for filtering the results in this way we need a reliable stable point in the area. Also, all interferograms must be unwrapped with regard to this point, which may cause problems if this point has low coherence or is enclosed by incoherent pixels in a small area. For the Komořany site, two stable points are required, each in the processed part of the scene.

Phase unwrapping is the most requiring and sensitive step of the interferometric processing. Phase ambiguities are estimated in this step with regard to the neighbouring pixels of the interferogram. However, estimation of the ambiguities with regard to other interferograms, not considering the spatial neighbourhood, showed to produce a spatially very discontinuous results, physically not evincible. We therefore decided to perform phase unwrapping independently for each interferogram and then estimate the ambiguities common to all pixels. There may be errors in the ambiguities originating from the errors in phase unwrapping, and the velocity model is better able to deal with them, due to the fact that it has smaller number of parameters.

4.2 Conclusion and future work

According to the cited figures, the Most site appears to be stable. An interesting fact here is that the areas with high image magnitude (the center of the scene, magnitude is the intensity component of figure 4.3), which coherence should be better than the coherence of the other parts (see figure 4.10, appears mostly not to satisfy the Kolmogorov-Smirnov test. This may be even caused by the fact that the deformations happen here, but the phase unwrapping is errorneous or the ambiguities are estimated badly (let us remind here that those ambiguities which apply for most pixels, are then selected).

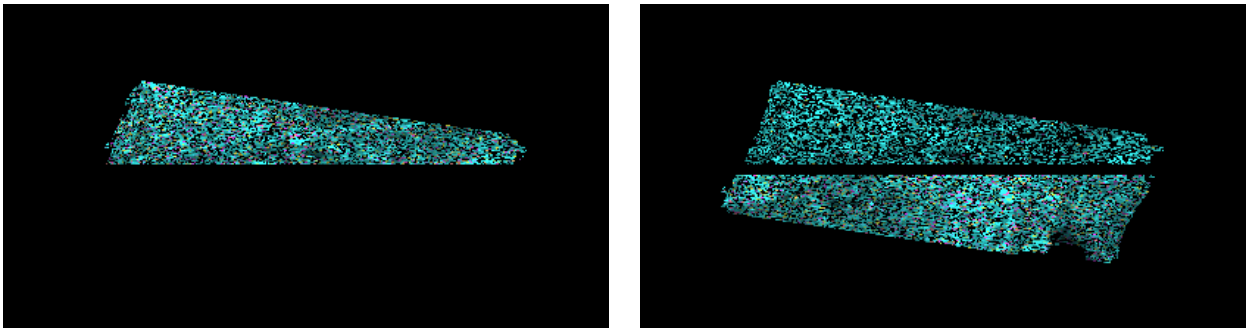

Figure 4.11: Geocoded (orthogonal latitude-longitude projection) deformation velocities of the upper and lower part of the Komořany site. The colorscale is displayed in figure 4.7.

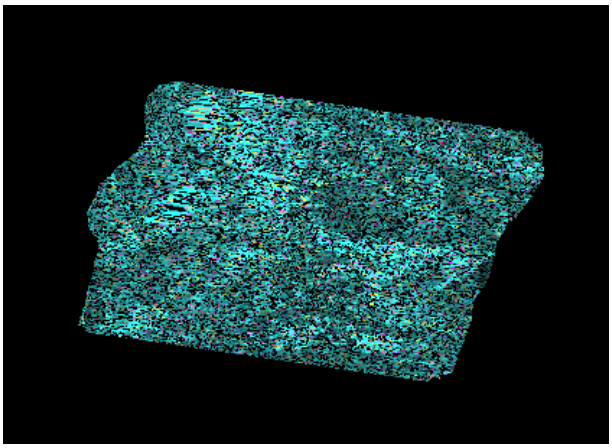

Figure 4.12: Geocoded (orthogonal latitude-longitude projection) deformation velocities of the Most site. The colorscale is displayed in figure 4.7.

The Komořany site appears to be almost stable. The left side of both parts of the site seems to be slightly deformed, however, this is quite invisible in figure 4.1.

Also the Louny site appears to be stable. Due to the large velocity standard deviations, the results in the areas which look to be unstable are irreliable. In addition, the coherence is not good in these areas.

In future, we plan to process more data in each locality. To improve the accuracy of the method, other scenes may be joined to the stack; however, to improve the reliability, the additional data may be processed separately to give independent results.

There are four stacks of data available, one of them was already processed for the three sites. The second stack contains the same area, the other two stacks contain only the eastern part of the area. Unfortunately, there are no data from ascending track available. Ascending track data would be a good source of independent data, allowing to prove the deformations and to assess them in 3D.

Another source of independent data would be an in-situ geodetic measurements, but currently, this type of data is not available. Geodetic measurements are performed only in certain areas, usually already deformed.

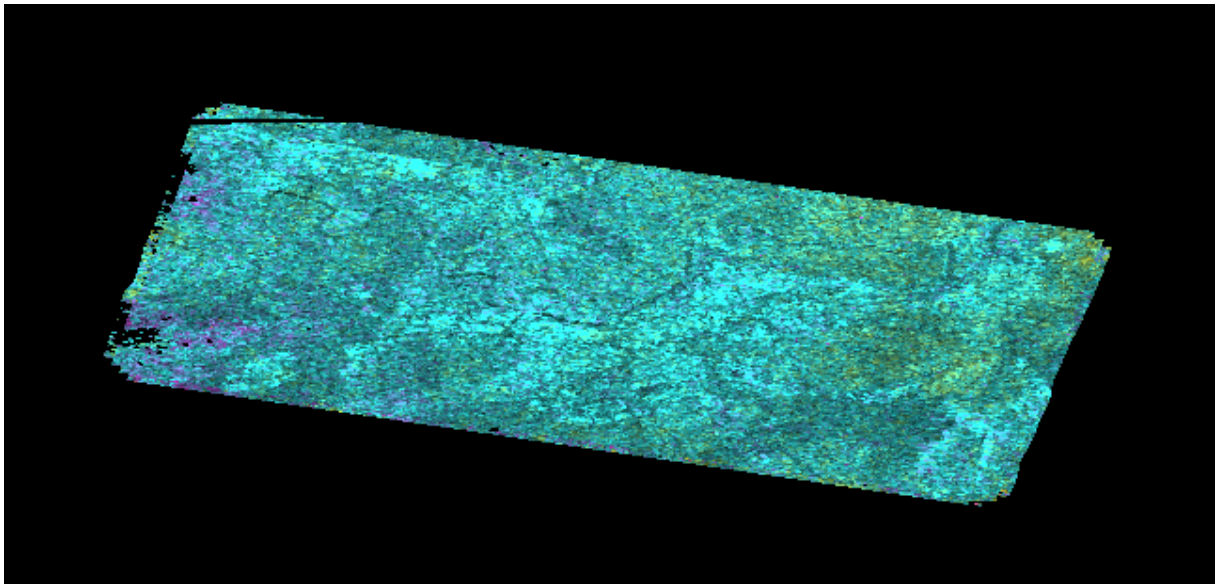

Figure 4.13: Geocoded (orthogonal latitude-longitude projection) deformation velocities of the Louny site. The colorscale is displayed in figure 4.7.

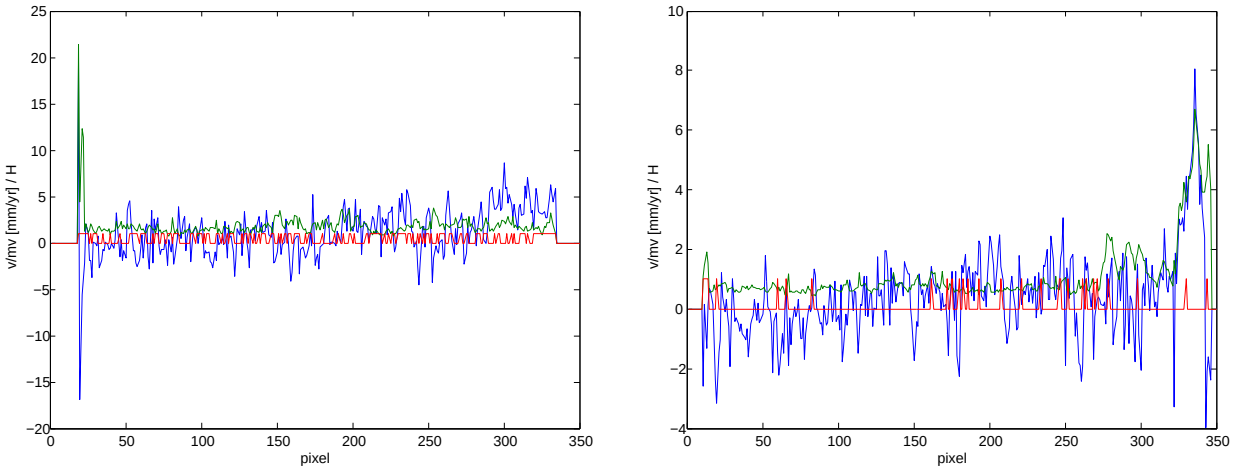

a b

Figure 4.14: Louny site - deformation velocities (blue line), their standard deviations (green line) and Kolmogorov-Smirnov test results (red line) for line 193 (a) and 78 (b). K-S test results are 1 for valid pixels and 0 for invalid ones. At the areas which look to be deformed, the velocity standard deviation are much larger than in other areas. The K-S test is usually unsatisfied in these areas.

Bibliography

[1] P. Berardino, G. Fornaro, R. Lanari, and E. Sansosti. A new algorithm for surface deformation monitoring based on small baseline differential SAR interferograms. *IEEE Transactions on Geoscience and Remote Sensing*, 40(11):2375–2383, 2002.

[2] R. M. Goldstein and C. L. Werner. Radar interferogram filtering for geophysical applications. *Geophysical Research Letters*, 25(21):4035–4038, nov 1998.

[3] M. Hampacher and V. Radouch. *Teorie chyb a vyrovnávací počet*. Vydavatelství ČVUT, 2000.

[4] R. Hanssen and S. Usai. Interferometric phase analysis for monitoring slow deformation processes. In *florence97*, ESA SP-414, pages 487–491, 1997.

[5] R. F. Hanssen. *Radar Interferometry: Data Interpretation and Error Analysis*. PhD thesis, Delft University of Technology, 2001.

[6] S. Usai. A least squares database approach for SAR interferometric data. *IEEE Transactions on Geoscience and Remote Sensing*, 41(4):753–760, apr 2003.